



ELSEVIER

Available online at [www.sciencedirect.com](http://www.sciencedirect.com)

SCIENCE @ DIRECT®

International Journal of Thermal Sciences 42 (2003) 665–676

International  
Journal of  
Thermal  
Sciences

[www.elsevier.com/locate/ijts](http://www.elsevier.com/locate/ijts)

# Isothermal and non-isothermal oil–water flow and viscous fingering in a porous medium

Tanuja Sheorey, K. Muralidhar \*

*Department of Mechanical Engineering, Indian Institute of Technology Kanpur, Kanpur 208016 UP, India*

Received 22 March 2002; accepted 13 August 2002

## Abstract

Immiscible flow of heavy oil in a porous formation by high temperature pressurized water has been numerically studied. The physical region is a square domain in the horizontal plane with low and high pressure points at the opposite corners along one of the diagonals. Water, the invading fluid, when introduced at high pressure displaces the *in situ* oil towards the low pressure production zone. The extent of displacement of oil by water through the porous medium in a given amount of time and the appearance of preferential flow paths (*fingers*) is the subject of the present investigation. The resistance to water–oil movement arises from the viscous forces in the fluid phases and the capillary force at their interface. Based on their relative magnitudes, various forms of displacement mechanisms can be realized. As the viscosity ratio of heavy oil to water is large, viscous forces in the oil phase become dominant and constitute the major factor for controlling the flow distortions in the porous formation. A mathematical model that can treat the individual fluid pressures, capillary effects and heat transfer has been employed in the present work. A fully implicit, two-dimensional numerical model has been used to compute the pressure and temperature fields. The domain decomposition technique has been adopted in the numerical solution since the problem is computationally intensive. Naturally occurring oil-rich reservoirs to which the present study is applicable are inhomogeneous and layered. A qualitative study has been carried out to explore the effect of permeability variations on the flow patterns. Numerical calculations show that non-isothermal effects as well as layering promote the formation of viscous fingers and consequently the sweep efficiency of the high pressure water front. © 2003 Éditions scientifiques et médicales Elsevier SAS. All rights reserved.

*Keywords:* Immiscible displacement; Oil–water system; Porous medium; Numerical simulation; Viscous fingering

## 1. Introduction

The displacement of oil by pressurized water in an isotropic porous medium has been numerically modelled in the present study. The configuration adopted for analysis is motivated by its application to enhanced oil recovery (EOR) from natural reservoirs. The focus of the study is towards understanding the performance of thermal EOR methods, when the injected water is at temperature higher than that of the *in situ* oil.

Owing to heterogeneities in the porous formation or those in the pressure and temperature fields, the flow pattern in the reservoir can become quite complex. A pattern that is particularly disadvantageous is the appearance of single or multiple fingers in the physical domain. The fingering phenomenon refers to the bypassing of the resident fluid

such as oil by an invading fluid, such as water [1]. The finger in turn contains the bulk of the invading fluid. This definition encompasses the consequences of instability of the fluid interfaces caused by viscous forces, capillary forces and permeability distributions. Heterogeneities in the porous medium add to the complexity of the nonlinear fluid–fluid interactions in multiphase flow. The oil–water flow patterns in uniform and layered reservoirs and the effect of non-isothermal water injection have been investigated in the present work.

Fingering phenomena in oil–water flow under isothermal conditions have been studied by several authors. A single discontinuity separating two homogeneous rock layers of different, constant permeabilities has been studied in [2]. The authors have reported that the regions of local maxima in the permeability field serve as nuclei for growth of fingers in porous media. The nonlinear mechanisms involved in viscous fingering have been considered in [3], wherein the stability characteristics of the flow field was seen to depend on the mobility ratio of the two phases. Further, the nonlinear

\* Corresponding author.

*E-mail address:* [kmurli@iitk.ac.in](mailto:kmurli@iitk.ac.in) (K. Muralidhar).

**Nomenclature**

$c$	specific heat capacity . . . . . $\text{J}\cdot\text{kg}^{-1}\cdot\text{K}^{-1}$	$\varepsilon$	porosity
$K$	absolute permeability of the formation . . . . . Darcies or $\text{m}^2$	$\Gamma$	interface boundary between the subdomains
$k_{ri}$	relative permeability of the $i$ th phase	$\mu_i$	dynamic viscosity of the $i$ th phase . . . $\text{N}\cdot\text{m}\cdot\text{s}^{-1}$
$k_h$	thermal conductivity of the porous medium . . . . . $\text{W}\cdot\text{m}^{-1}\cdot\text{K}^{-1}$	$\lambda_i$	mass flux of the $i$ th phase, $= -k_{ri} \partial p_i / \partial x$
$L$	size of the physical domain . . . . . m	$\rho_i$	density of the $i$ th phase . . . . . $\text{kg}\cdot\text{m}^{-3}$
$n, m$	grid points along the $x$ and $y$ axes	$\theta$	interface convergence parameter in Schwarz's algorithm
$p_{cow}$	capillary pressure between oil and water phases . . . . . $\text{N}\cdot\text{m}^{-2}$	$\Omega, \partial\Omega$	physical domain and its boundary
$p_i$	phase pressure of the $i$ th phase . . . . . $\text{N}\cdot\text{m}^{-2}$	$\xi_i$	compressibility of the $i$ th phase . . . . . $\text{Pa}^{-1}$
$S_i$	saturation of the $i$ th phase in the porous region	<i>Superscript</i>	
$t, \Delta t$	time and time step . . . . . s	$k$	current time step
$T$	temperature . . . . . $^{\circ}\text{C}$	<i>Subscript</i>	
$T_f$	temperature of rock formation . . . . . $^{\circ}\text{C}$	f	formation
$u, v$	Darcy velocity . . . . . $\text{m}\cdot\text{s}^{-1}$	$i$	index representing oil or water
$x, y$	Cartesian coordinates . . . . . m	inj	injection
<i>Greek symbols</i>		o	oil
$\alpha$	interface convergence parameter in Uzawa's algorithm	ref	reference
$\beta_i$	expansivity of the $i$ th phase . . . . . $^{\circ}\text{C}^{-1}$	R	solid phase of the porous formation
		w	water

behaviour of the fingers became prominent at a later time. Specifically, a few dominant fingers were seen to shield the growth of other fingers. A general procedure for the scale-up of heterogeneous models has been proposed in [4]. The method captures both the nature of the displacement process as well as the breakthrough of the displacing fluid.

The displacement of oil by water through porous media at the level of the interconnected pores has been previously studied. Dias and Payatakes [5] have discussed the basic forms of microdisplacement through a random porous formation. The limiting values of the dimensionless numbers characterizing various forces have been identified in this work. These results have been further tested through experiments on micromodels [6].

In the presence of both viscous and capillary forces, immiscible displacement of two fluids in a porous medium can exhibit one of the three forms: stable displacement, viscous fingering, and capillary fingering [7]. In stable displacement the driving force arises from the viscosity of the injected fluid. Capillary effects at the interface are of secondary importance. The resulting front is flat with irregularities restricted to the pore level. In viscous fingering, the viscosity of the resident fluid is the predominating influence. Capillary effects are once again negligible. The capillary fingering phenomenon arises from large forces of surface tension, particularly when the viscosity of the fluids involved (for example, air and water) is small.

The present investigation is concerned with the displacement mechanisms in oil–water flow in a porous medium. The factors destabilizing the front movement are variations in the

absolute permeability and temperature differences between the injected water and the resident oil. The geometry considered is a quarter five-spot region, referred subsequently as the 2-spot problem. Flow of oil resulting from water injection and the areal sweep of the injected fluid in the porous formation have been studied.

## 2. Mathematical model

The physical region being analyzed has been chosen from the literature on enhanced oil recovery. It is a square domain of size  $L$  in the horizontal plane with an injection and a production well at the opposite corners along one of the diagonals [2,8,9]. The remaining boundaries are planes of symmetry. A regular Cartesian grid has been used for the numerical simulation of the oil recovery process with a suitable adjustment for the well shapes. The regions close to the injection and production wells have been accounted for by refining the grid locally and specifying appropriate boundary conditions. Fig. 1 shows a  $101 \times 101$  grid on a  $10 \text{ m} \times 10 \text{ m}$  domain. The circular shape of the injection and the production wells has been represented on this grid by 11 nodes, spaced in a manner to make it close to a quarter of a circle. The physical domain is a porous medium, filled with oil at a prescribed initial saturation of 0.8, the rest being water. Water is injected at a pressure higher than that of the formation through the injection well. A mixture of oil and water is recovered at the production well.

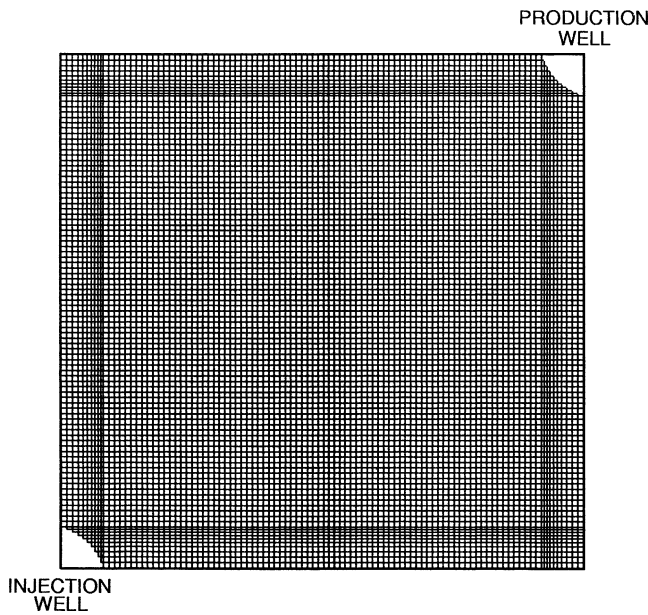


Fig. 1. Cartesian grid of 101 × 101 on a 10 m × 10 m domain.

The mathematical formulation of the conservation equations governing oil–water flow in a porous medium is summarized below [1,8,10–13]:

**Conservation of mass:** The mass balance equation for each of the phases namely oil and water are:

$$\frac{\partial}{\partial t}(\varepsilon S_i \rho_i) + \nabla \cdot (\rho_i u_i) = 0 \quad i = \text{oil, water} \quad (1)$$

**Momentum:** The momentum equations in the form of the generalized Darcy’s law for each phase are written as:

$$u_i = -\frac{K k_{ri}}{\mu_i} \nabla p_i \quad (2)$$

where  $K$ , the absolute permeability of formation can be a space-dependent property. Eqs. (1) and (2) governing transient two-phase flow through a heterogeneous but isotropic porous medium can be combined in terms of the phase pressures to yield:

$$\begin{aligned} -S_o \beta_o \frac{\partial T}{\partial t} + S_o \xi_o \frac{\partial p_w}{\partial t} - \frac{dS_w}{dp_{c_o,w}} \left[ \frac{\partial p_o}{\partial t} - \frac{\partial p_w}{\partial t} \right] \\ = \frac{1}{\rho_o} \nabla \cdot \left[ \frac{K k_{ro} \rho_o}{\mu_o \varepsilon} \right] \nabla p_o \end{aligned} \quad (3)$$

$$\begin{aligned} -S_w \beta_w \frac{\partial T}{\partial t} + S_w \xi_w \frac{\partial p_w}{\partial t} - \frac{dS_w}{dp_{c_o,w}} \left[ \frac{\partial p_o}{\partial t} - \frac{\partial p_w}{\partial t} \right] \\ = \frac{1}{\rho_w} \nabla \cdot \left[ \frac{K k_{rw} \rho_w}{\mu_w \varepsilon} \right] \nabla p_w \end{aligned} \quad (4)$$

**Conservation of energy:** Assuming local thermal equilibrium among contiguous phases, the equation for conservation of energy in two-phase flow can be expressed as [8]:

$$\frac{\partial T}{\partial t} + UT_x + VT_y = \frac{K_h}{\sigma_T} \nabla^2 T \quad (5)$$

where

$$U = \frac{u_o \rho_o c_o + u_w \rho_w c_w}{\sigma_T}$$

$$V = \frac{v_o \rho_o c_o + v_w \rho_w c_w}{\sigma_T}$$

$$\sigma_T = \varepsilon(1 - S_w) \rho_o c_o + S_w \rho_w c_w + (1 - \varepsilon)(\rho c)_R$$

and  $T$  is the local volume-averaged temperature.

Eqs. (3) and (4) for oil and water pressures and Eq. (5) for temperature form a closed system of equations. The above equations have been solved simultaneously for oil and water pressures and the average temperature. These equations have to be supplemented by constitutive relations of the form:

$$k_{rw} = k_{rw}(S_w)$$

$$k_{ro} = k_{ro}(S_w)$$

$$p_o - p_w = p_{c_{ow}}(S_w)$$

$$S_o + S_w = 1$$

$$\frac{\rho_i}{\rho_{i,\text{ref}}} = 1 + \xi_i(p_i - p_{i,\text{ref}}) - \beta_i(T - T_{\text{ref}})$$

$i = \text{oil, water}$

Detailed forms of these relations have been adapted from [8] and also reported by the authors elsewhere [13].

Unique solutions for the flow and the thermal field are obtained by supplying suitable initial and boundary conditions. These correspond to a specified initial water pressure, saturation and temperature in the physical domain. Dirichlet boundary conditions can be specified at the injection well in terms of pressure, saturation and temperature. These conditions are summarized below:

- $t = 0$ :  $S_w, p_w, T$  prescribed, all  $x$  and  $y$ ;
- At the injection point:  $S_w, p_w, T$  prescribed, all  $t$ .

Along the planes of symmetry, the gradient condition prevails as follows:

- $x = 0$  and  $L$ ;  $\partial T / \partial x = 0$  and  $\partial p_i / \partial x = 0$ ,
- $y = 0$  and  $L$ ;  $\partial T / \partial y = 0$  and  $\partial p_i / \partial y = 0, i = \text{oil, water}$ .

The numerical solution of the EOR problem experiences a growth of errors during long time integration. The errors are quite significant when large physical domains are simulated. The first manifestation of the errors is seen in the form of oscillations in the numerical solution of the oil–water equations. The origin of the oscillations and methods of control have been discussed previously by the authors [13]. In the present work, numerical oscillations were eliminated by enforcing a Neumann condition of the form

$$\frac{\partial S_w}{\partial r} = 0$$

$$\frac{\partial T}{\partial r} = 0$$

at the low pressure point, namely the production well. Here  $r$  is the local radial direction.

### 3. Numerical solution

Several multi-phase oil recovery simulators have been reported in the literature [10–12]. A majority of them deal with isothermal conditions in the reservoir. They are based on the solution of the parabolic pressure equation and the hyperbolic water saturation equation. In the present work, the pressure–saturation approach has been replaced by the pressure–pressure formulation for the oil and water phases. This step was based on the expectation that the saturation equation would be quite stiff under the combined influences of fingering and thermal gradients. Additional advantages of the pressure–pressure formulation arise from the mathematical similarity of the pressure equations. It leads to an improved matrix structure of the discretized equations and permits the application of domain decomposition algorithms.

The oil and water pressure equations (3), (4) and the temperature equation (5) have been discretized in the present work using a finite difference scheme. Spatial derivatives are evaluated using central differencing. Time derivatives of the pressure equations are discretized using the forward difference formula. The scheme is fully implicit in time. However, the derivatives of temperature appearing in Eqs. (3) and (4) have been evaluated at the earlier time level. Water saturation has been obtained through the constitutive relation that relates  $S_w$  to the pressure difference  $p_{c_{ow}}$ .

For a  $n \times n$  grid in the physical domain, the discretized equations contain  $2n^2$  unknowns to be solved simultaneously for the oil and water pressures. Owing to the complexity of the two-phase model, a sparse-banded unsymmetric coefficient matrix is obtained from the linearized pressure equations. Repeated inversion of this matrix is one of the most computationally intensive steps of the calculation. Hence it has to be performed as efficiently as possible. In the present work, the preconditioned conjugate gradient (PCG) method has been employed for matrix inversion [14]. Preconditioning has been performed at every iteration of all the timesteps. It is based on the incomplete  $LU$  factorization of the coefficient matrix, formed by ignoring the possible fill-in outside the prescribed band. To reduce the matrix size, its bandwidth and to facilitate parallelization of the numerical algorithm, a domain decomposition algorithm has been employed in the present study [15]. The energy equation has been solved using an operator-splitting algorithm [16]. Here the advection step employs an analytical solution, while the diffusion step is solved by ADI.

Results presented in the following sections have been derived from a grid comprising of  $101 \times 101$  nodes covering a square region of 10 m size. The time step employed in the calculations was nominally 0.01 hour, being smaller ( $= 0.001$  hour) in the initial stages. Though a hyperbolic equation was not being solved, the cell Reynolds and Peclet numbers were consistently kept at values much below unity. For simplicity in counting the node numbers, the grid points lying within the well were also taken into consideration. The solution in the active portion of the physical domain was

not affected by these fictitious points. Typical convergence criteria employed in the calculations are  $1.0E-07\%$  in the PCG iterations and  $0.05\%$  in the nonlinearity iterations involving the phase pressures and temperature. All the computations were carried out on P-III, 800 MHz, 512 MB RAM machines. For a one hour simulation, the CPU time required was close to 36 hours (isothermal), and 20 hours (non-isothermal). The CPU times without domain decomposition were greater by a factor of three. Without preconditioning of the global stiffness matrix, convergence was not attained in any of the simulations reported in the present work.

The initial computer code for the present work was adapted from the earlier work of the authors [13]. The code has been validated against benchmark analytical solutions for diffusion and advection-diffusion problems on one hand, and the difficult oil-bank problem described in [8]. Selected calculations were carried out on a grid of  $121 \times 121$ . The results were seen to be identical to those obtained on the  $101 \times 101$  grid. A few calculations were also performed on a  $151 \times 151$  grid. Once again, the computed fields were quite similar to the coarser grid. Marginal differences were however seen in the saturation contours and the in the critical time instants at which fingering was initiated. The long-time solutions are however expected to be unaffected. Hence all results reported below have been derived on a  $101 \times 101$  grid.

### 4. Results and discussion

Results of the numerical simulation of enhanced oil recovery from a porous formation using a two-spot model are discussed in the present section. Results have been presented in terms of the distribution of pressure, water saturation and the phase averaged temperature. Oil recovery as a function of time also has been reported in the present work. The emphasis is on the displacement characteristics of the invading water front upto breakthrough, a state corresponding to the injected water reaching the production well. Numerical results have been presented for a homogeneous as well as a layered medium, under conditions of isothermal and non-isothermal injection of water. Of interest to the present study are the formation of fingers, their evolution with time, oil recovery and the accumulation of water at the production well. In this respect, the earlier work of the authors [13] can be viewed as a preliminary study of oil–water flow, with a focus on the numerical technique and the short duration trends in a homogeneous medium.

The pressure at the injection well is prescribed as 1.79 MPa, the initial formation and the production well pressures being 1.31 MPa. During isothermal injection, water is injected at the formation temperature of  $50^\circ\text{C}$ . In non-isothermal injection, the water temperature is held at  $100^\circ\text{C}$ . The nominal permeability of the formation is 132 Darcies ( $= 130 \times 10^{-12} \text{ m}^2$ ). Variation with respect to this value has

been considered for a layered medium. Constitutive relations as well as the fluid properties have been adopted from [8].

In order to visualize the flow field in a heterogeneous medium, a two-layer formation has been considered. The permeability ratio of the two layers is 3, the lower permeability region being adjacent to the injection well. It is to be noted that the governing equations (1)–(5) provide a volume-averaged description of the flow and hence permit only a macroscopic characterization of the heterogeneities in the porous formation. In view of a numerical approach adopted in the present work, permeability variations on the scale smaller than the grid size cannot be resolved [2,4].

4.1. Displacement processes during isothermal injection

Flow in homogeneous and layered formations under isothermal conditions is first discussed. The pressure contours in a homogeneous formation at initial and later times are shown in Fig. 2(a), (b). The pressure referred here is that of water, the oil pressure trends being practically identical. The main features for the pressure field include the attainment of a nearly steady pattern quite early in time, followed by small fluctuations later in response to the moving saturation front. Pressure contours for other configuration were found to be similar and have not been repeated. For the homogeneous formation, the pressure distribution is symmetric

about the main diagonal of the physical domain. This is adequately reflected in Fig. 2(a), (b). There is a marginal loss of symmetry in the saturation contours discussed below, a result that can be explained as follows: Water saturation is a function of the capillary pressure ( $p_o - p_w$ ), that is of the order of a few kilopascals (kPa). The individual pressures are themselves of the order of a few megapascals (MPa). Thus, small errors in the computed water and oil pressures can appear as a larger error in the capillary pressure and in turn, the water saturation.

Fig. 3(a), (b) show the displacement pattern for a homogeneous formation in terms of the water saturation contours plotted at time instants of 50 and 63 hours. For the initial one hour, the saturation front was seen to move radially outwards in a symmetric manner and has not been shown. During this period, the presence of the production well is felt and a two-dimensional pressure field as in Fig. 2(a) is established. It is to be expected that the gradient along the direction of the central diagonal is dominant, leading to a distortion of the purely radial shape of the saturation contours. Over a period of 8 hours, the oil–water interface was seen to move faster along the diagonal joining the injection and the production wells, leading to the incipient appearance of the first finger. Continued injection beyond this time showed front movement to be slow, and the outer saturation contour to be disturbed (Fig. 3). The spatial fluctuations in Fig. 3 are of

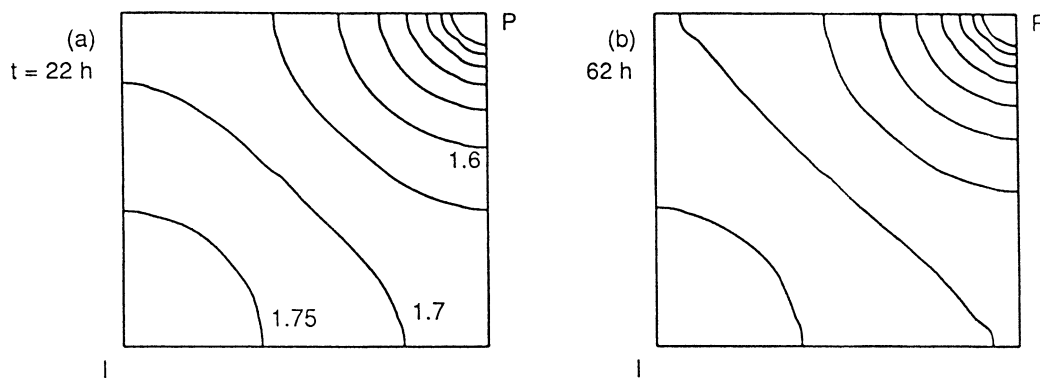


Fig. 2. (a), (b). Isothermal injection: Water pressure contours in a homogeneous formation at two time instants. The maximum water pressure shown is 1.75 MPa close to the injection well, and the minimum is 1.35 MPa close to the production well. The pressure increment is 0.05 MPa.

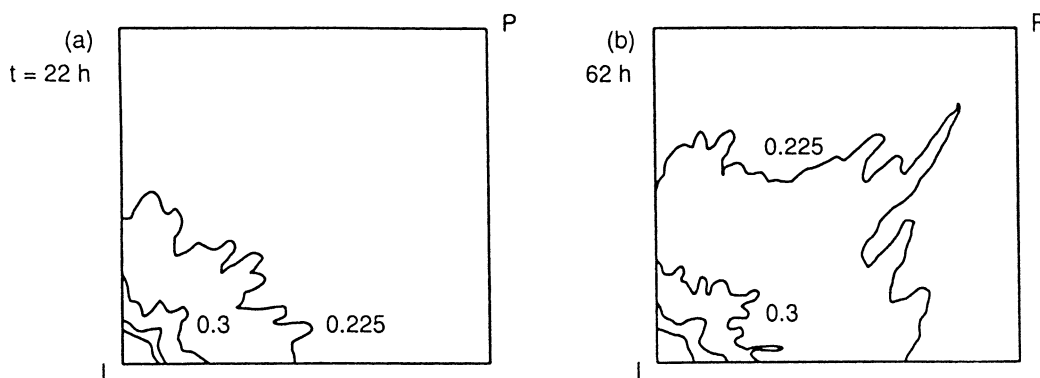


Fig. 3. (a), (b). Isothermal injection: Evolution of water saturation contours in a homogeneous formation at two time instants. Maximum water saturation shown is 0.5 and occurs close to the injection well.

two types: multiple fingers and superimposed wiggles. By tracking the saturation contours of other magnitudes, it was found that the multiple but low amplitude fingers were temporal features that formed periodically with time. These are not true fingers in the sense that not a single one was seen to grow in time to become active enough to reach the production well. The front therefore remained stable around the central finger. From an engineering viewpoint, the invading fluid was seen to move progressively through the domain and no preferential paths were set up. The net effect is that of a greater swept area and oil recovery, though requiring a long time period.

Visualization of fingering in a laboratory-scale experimental setup during isothermal miscible displacement has been reported in [9]. The mobility ratio in the referred experiments was small, being in the range of 4–25. This is to be contrasted with a value of 1800, employed in the present study. Flow visualization experiments were conducted in a porous medium constructed with glass beads. It was observed that a prominent central finger (with superimposed wiggles) could form in the apparatus even in the absence of an inhomogeneity in the permeability field. The numerical simulation with the present code and the appropriate mobility ratio was seen to reproduce the experimental patterns quite well.

The isothermal results of immiscible displacement can be interpreted as follows. Water leaves the injection well radially, and is redistributed later in the porous medium depending on the nature of heterogeneity in the pressure field. Numerical results show that the evolution of the pressure field is marked by two time scales, that are distinctly separated. The basic pressure field is established quite rapidly and the front movement occurs in response to this distribution. Over a longer time scale, the flow in turn modulates the pressure field, though these changes are local and of a smaller magnitude. In a homogeneous medium, the pressure field continues to be non-uniform, and the diagonal joining the injection and the production wells is necessarily the path of least resistance. This can however be disturbed when the water is injected at a higher temperature (Section 4.2).

Saturation contours for oil–water flow in a layered formation is considered next. The porous region comprises of two distinct permeability layers of equal thickness, the permeability ratio being equal to three. The high permeability zone is located closer to the production well in Fig. 4, while it is adjacent to the injection well in Fig. 5.

As in the case of the homogeneous region, the oil–water front in Fig. 4 starts with a nearly radial shape for a time upto 3 hours. Over this time period, the overall pattern of

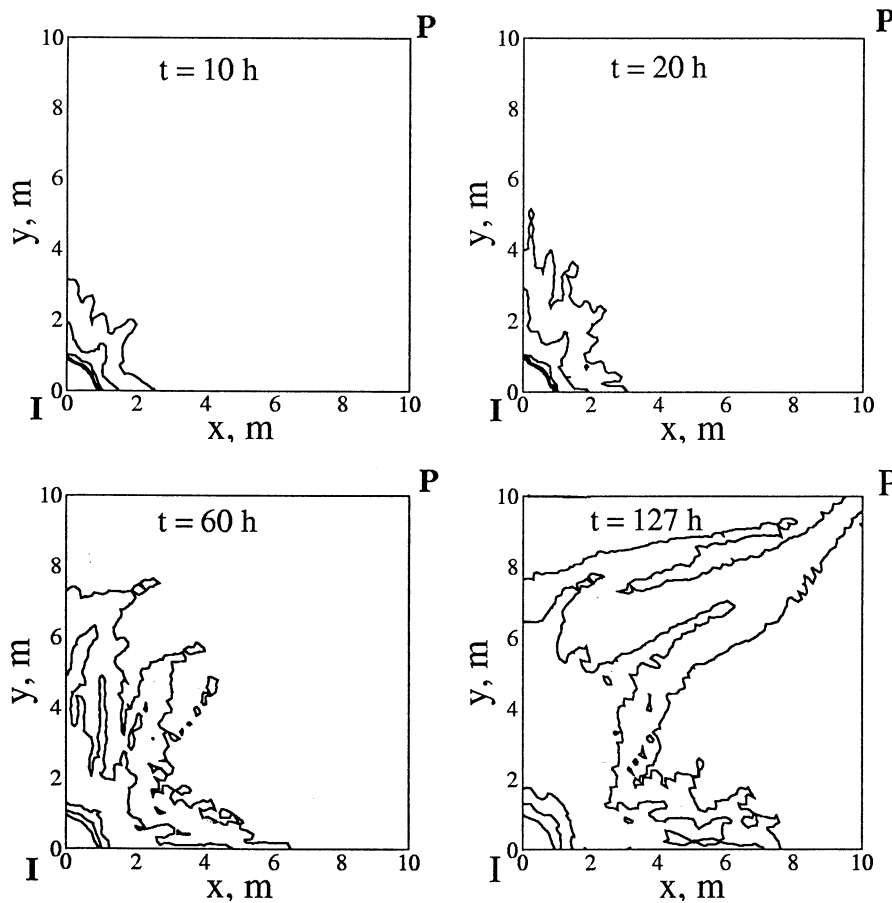


Fig. 4. Isothermal injection: Evolution of water saturation contours with time in a formation with the high permeability layer near the production well.

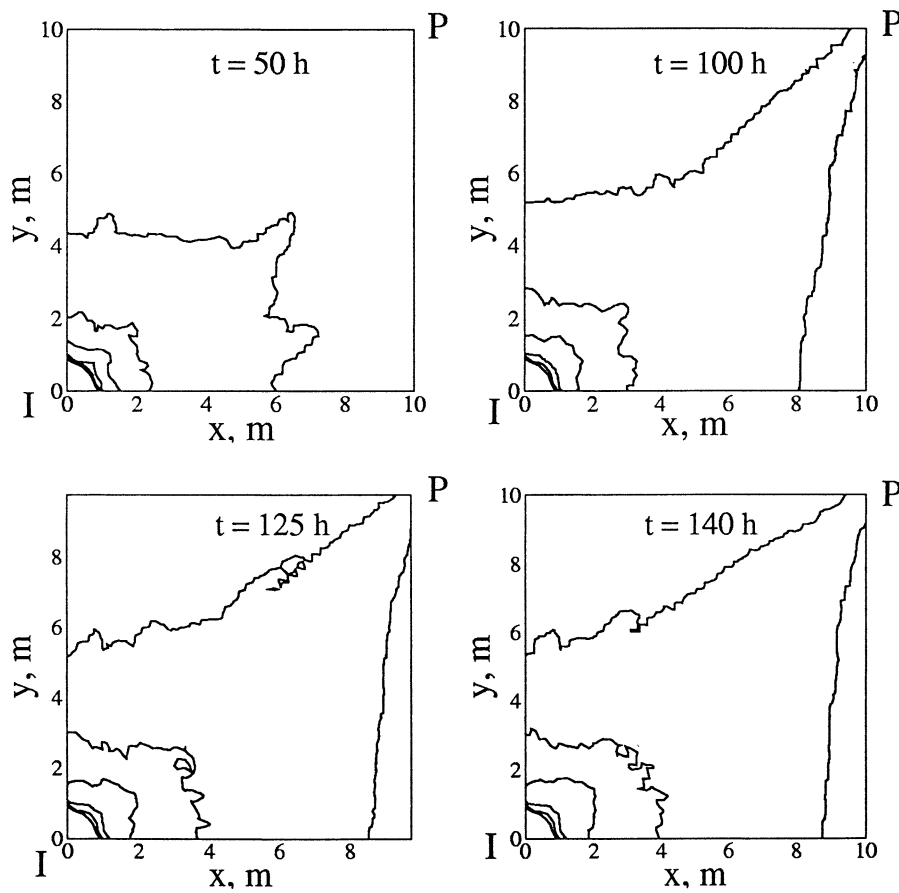


Fig. 5. Isothermal injection: Evolution of water saturation contours with time in a formation with the high permeability layer near the injection well.

the pressure gradient is established. Owing to the presence of the high permeability region the effective resistance to the front movement is lowered. On the other hand the permeability distribution in the formation ensures that the resistance to the movement of the displaced fluid in the radial direction is not a minimum, and alternative routes exist. As a result, the front moves with a greater speed towards the high conductivity zone along the left side. The consequence is that the injected water bypasses the resident oil along the way. Fig. 4(a) shows the growth of several distinct fingers at  $t = 10$  hours. The active fingers grow in size with time. The growth is accompanied by several secondary phenomena. These include the bifurcation of the finger tip and droplet formation. Fig. 4(b) at  $t = 20$  hours displays the phenomenon of tip-splitting at the central finger along the main diagonal. The edges of the tip move faster than the tip centre leading to the bifurcation of the finger (Fig. 4(c)). Additional phenomena that come into the picture at later times are pinch-off resulting in an isolated droplet of water. Multiple fingers now move towards the production well at varying speeds. Fig. 4(c), (d) show that it is possible for the moving fingers to merge, leading to a single dominant finger. In addition, the fingers formed along the boundaries of the physical domain become active at a later time and spear directly towards the production well, while the central finger is still not clear of the low permeability zone.

The saturation contours in a formation where the high permeability layer is adjacent to the injection well are shown in Fig. 5(a), (d). The migration of water along the high permeability layer, followed by appearance of stable finger are to be seen. The lower permeability layer adjacent to the production well is thus seen to stabilize the oil recovery process. A direct calculation of the total amount of oil displaced through the production well over a period of 140 hours showed the following: The presence of a low permeability region next to the production well lowers the amount of oil recovered in comparison to the homogeneous formation. The low permeability region next to the injection well shows a significant increase in the oil recovered. These results directly follow from the water saturation contours of Figs. 2–5.

#### 4.2. Displacement processes during non-isothermal injection

The influence of hot water injection on oil–water displacement in homogeneous and heterogeneous formations is presented below.

Flow in a homogeneous formation is taken up first. As in isothermal injection, the initial movement of the saturation front is purely radial. Simultaneously, a thermal front progresses from the injection to the production well.

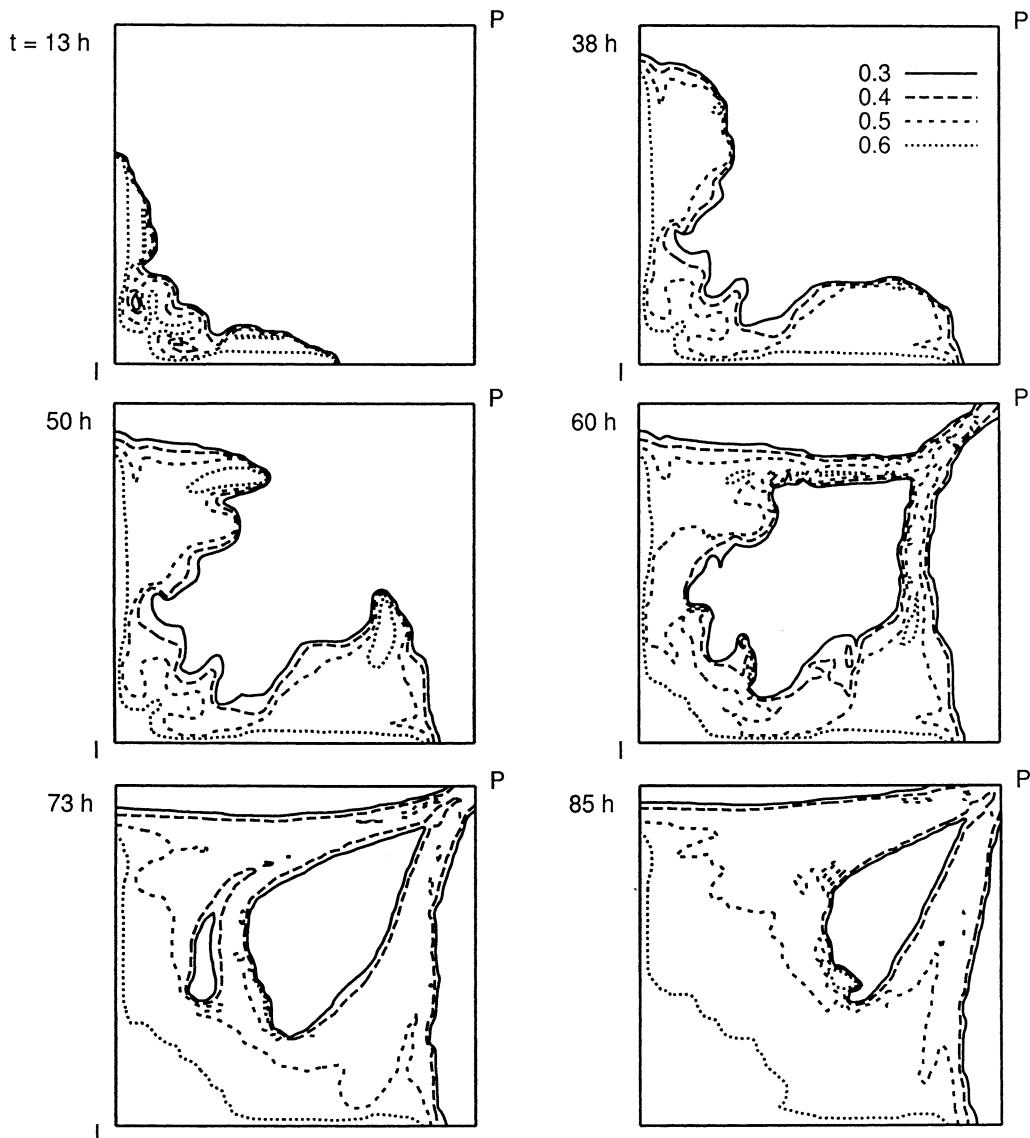


Fig. 6. Non-isothermal injection: Evolution of water saturation contours with time in a homogeneous formation.

The primary influence of the thermal front on oil–water displacement is through a reduction in the viscosity of oil in the vicinity of the thermal front. This can substantially lower the resistance to fluid displacement, resulting in momentarily high front speeds. It is possible for the fluid front to move faster than the thermal front and reach a location where the resident fluid just beyond the oil–water interface has a lower temperature and hence a higher viscosity. This situation can result in a lowering of the front speed on one hand, and the formation of by-pass fingers along the sides of the physical domain, on the other. The non-uniform movement of the oil–water interface is a characteristic feature of non-isothermal injection.

The rapid movement of the oil–water front owing to a lowered oil viscosity is seen at  $t = 8$  hours in Fig. 6(a). Aided by the reduced effective viscosity of the two phases and a dominant pressure gradient along the main diagonal of the physical domain, the front movement is radially

outwards, with the displacement being higher along the diagonal axis. The percentage oil recovered was calculated to be 3.57 at  $t = 12$  hours as against 1.07 for isothermal injection. This is indicative of the additional oil recovered at early times by non-isothermal injection. The rapid movement of the oil–water front brings it to a location where the local temperature is unaffected by the hot water injection. These regions continue to offer high resistance to oil–water flow. The combination of the displaced oil and that present in the formation results in the accumulation of oil (Fig. 6(b), (c)). The pattern of distribution of resistance to flow at this time instant is such as to promote the bypass of the invading fluid from the sides. In Fig. 6(c), (d), two side lobes can be observed, reaching the boundaries of the domain. At  $t = 46$  hours, Fig. 6(e) there is a clear evidence of the build-up of the saturation of the invading fluid at the tip of side lobes, leading eventually to formation of fingers (Fig. 6(f)). The porous formation being homogeneous the patterns re-

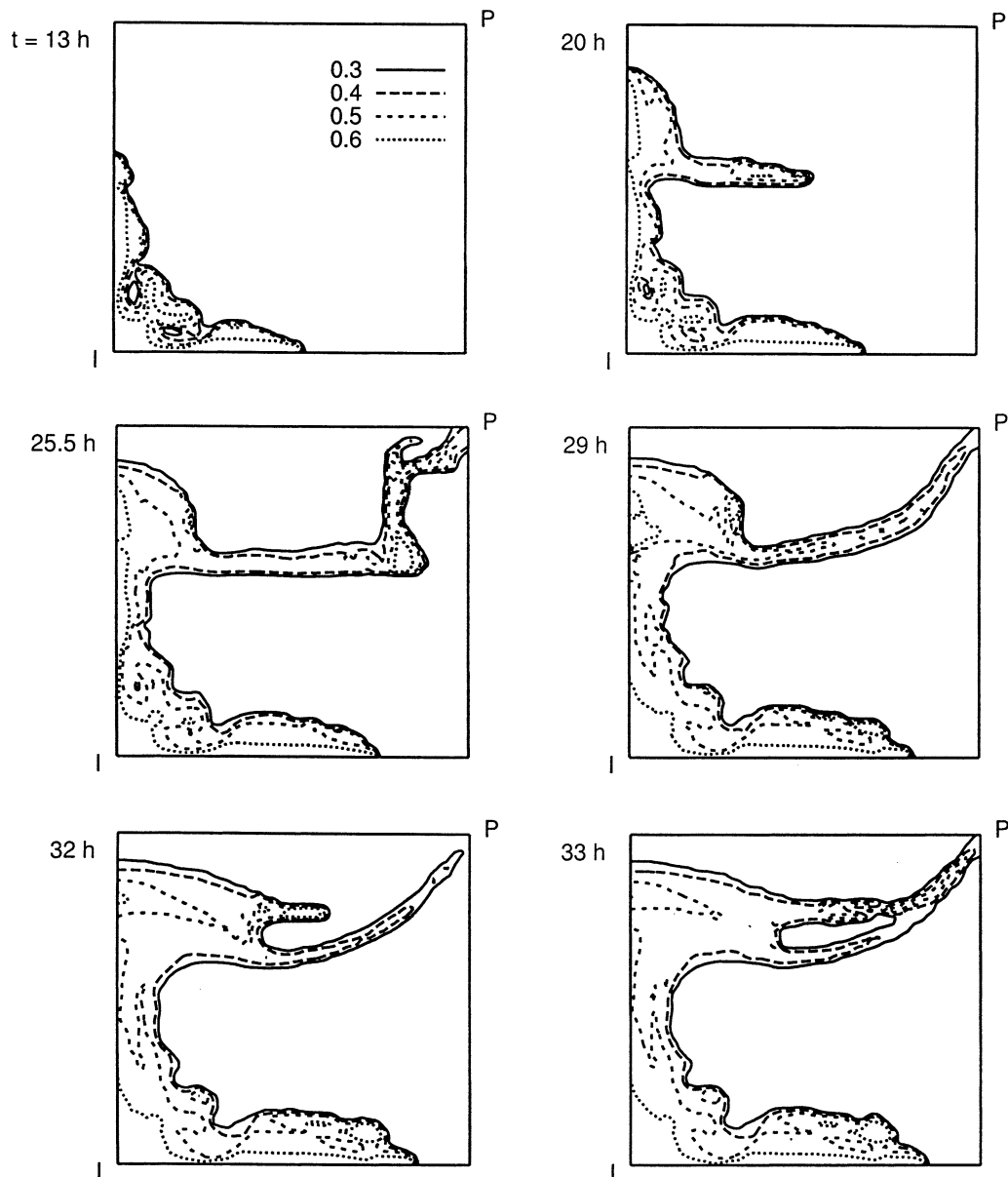


Fig. 7. Non-isothermal injection: Evolution of water saturation contours with time in a layered formation (high permeability layer near the production well).

main symmetric with respect to the main diagonal for all time. The percentage oil recovery for isothermal and non-isothermal injection at the end of 50 hours were calculated to be 3.01 and 12.28, respectively. Despite the accumulation of oil along the main diagonal, the formation of bypass fingers contributes to the increase in oil recovery, over and above the isothermal value.

Flow through the layered formation with the permeability contrast as in the isothermal injection method is discussed next. For definiteness, the high permeability zone is located near the production well. The displacement patterns initially evolve in almost the same manner as in the homogeneous formation. Differences are to be seen when the front reaches the high permeability zone ( $t = 13$  hours, Fig. 7(a)). The growth of a single finger can be observed at the first location

of the high permeability zone, which eventually grows to a dominant finger as shown in Fig. 7(b). Beyond this time the symmetry of the displacement pattern is lost. The invading fluid (namely, water) having found an environment of lower resistance moves rapidly towards the production well (Fig. 7(c), (d)). As a result, the water saturation increases everywhere within the finger. The appearance of a prominent finger in the high permeability zone of the formation is quite similar to the channeling phenomenon reported in the hydrological studies of fractured porous media.

The secondary phenomena associated with fingering during isothermal injection are also to be observed during non-isothermal injection. At  $t = 22.5$  hours, the broadening of the tip of the finger is seen. The tip bifurcates at a later time of  $t = 23$  hours. This is followed by a pinch-off

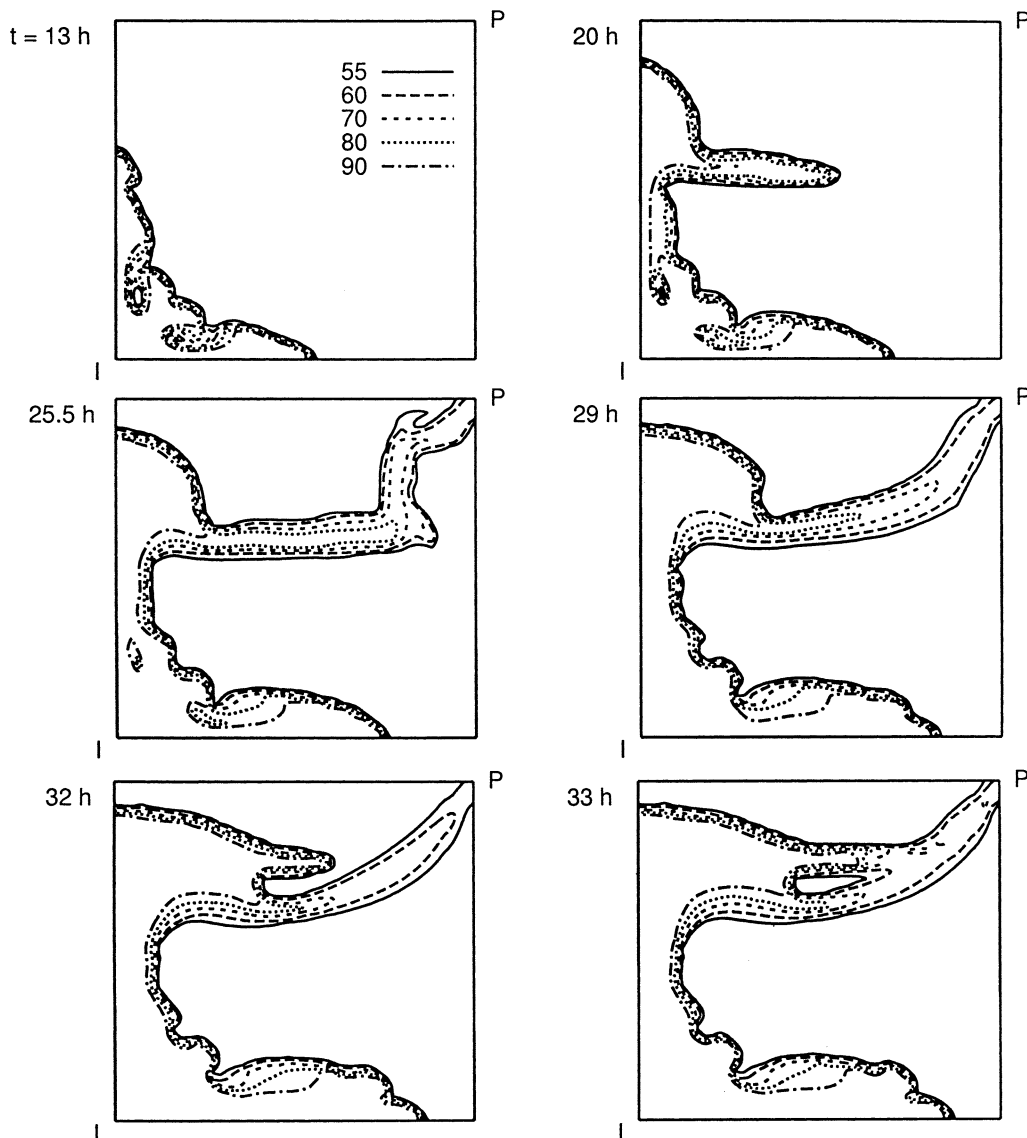


Fig. 8. Non-isothermal injection: Evolution of temperature contours with time in a layered formation (high permeability layer near the production well).

(namely, droplet formation that flows into the production well), and results in the termination of the cycle of finger movement. The next cycle commences at  $t = 32$  hours, Fig. 7(e), (f), with the growth of the second dominant finger channeling towards the production well.

The sequence of events described above is vividly brought out in terms of the temperature field in Fig. 8(a)–(f).

#### 4.3. Interpretation of displacement patterns

The present work is restricted to a class of flows where the viscosity contrast is quite high, leading to instabilities that are viscous (rather than capillary) in origin. The main observations emerging from Figs. 2–8 can be summarized as follows. During isothermal injection, symmetric patterns of the saturation front are observed in a homogeneous formation. The movement of the saturation front is quite slow. The disturbances superimposed on the front are localized. Since

no prominent fingers form, the displacement takes place uniformly leading ultimately to a high sweep efficiency, low a rate of oil recovery. For a layered formation, permeability contrast makes a significant contribution to the flow pattern. When the high permeability zone is adjacent to the injection well, a considerable part of the displacement takes place along a preferential path set up by the viscous fingers. Over a long period of injection, a considerable portion of the oil available in the formation is bypassed and leads to a poor sweep efficiency. When the high permeability zone is next to the production well, the sweep efficiency is significantly improved. In non-isothermal injection, the viscosity of crude oil is sharply reduced with increasing temperature. This factor promotes the formation of fingers and affects the displacement process to such an extent that the sweep efficiency is once again lowered. The combination of layering and thermal effects lead to large structural changes in the flow field. Results show that the flow bypasses the oil-rich

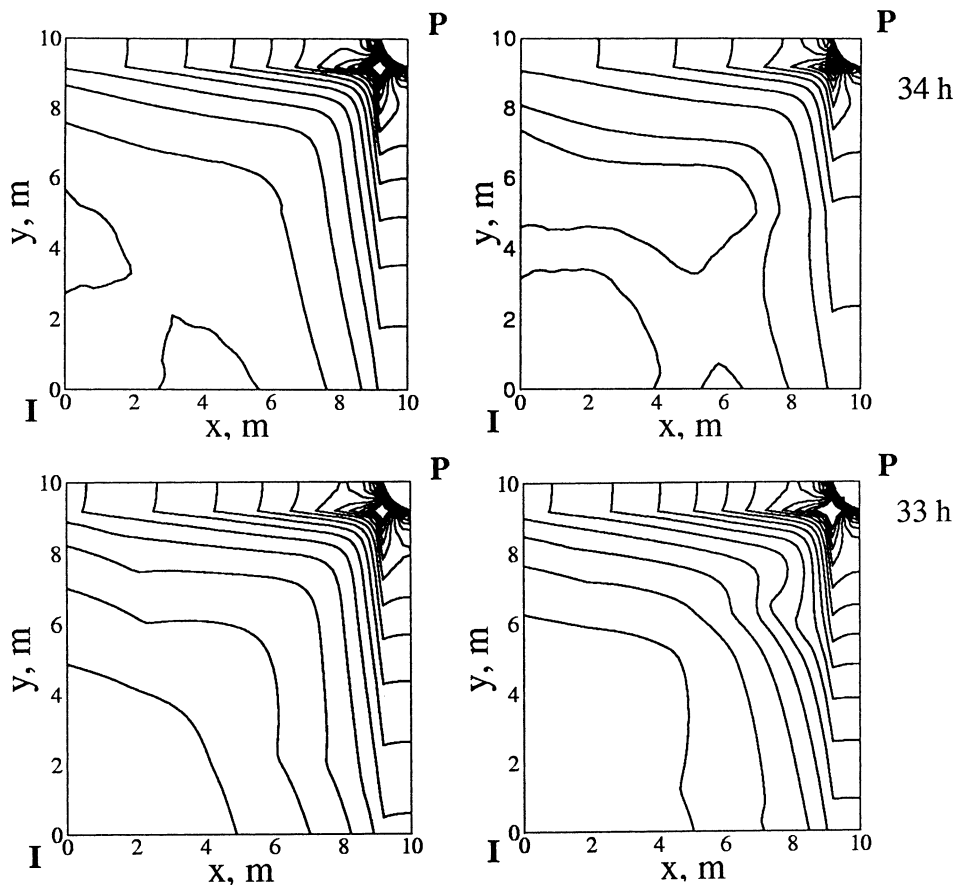


Fig. 9. Pressure gradient contours in a homogeneous (left column) and a layered formation (right column). Top row is for isothermal injection; bottom row for non-isothermal injection.

regions by the formation of water channels that reach the production well quite early. The channels subsequently get pinched off from the rest of the finger, and lead to the formation of a pool that is drawn into the production well. The channel once again grows with time, thus enforcing a degree of periodicity to the flow field.

The flow patterns in the homogeneous and heterogeneous formations with isothermal and non-isothermal injection can be discussed in terms of physical mechanisms as follows. The flow through the porous formation essentially takes place from the injection well to the production well under the influence of the following factors:

- (1) Macroscopic heterogeneity in permeability;
- (2) Phase viscosities and interfacial tension;
- (3) Wettability;
- (4) The pressure distribution.

In the present work, water is taken to be the wetting phase with respect to the solid matrix, while oil and water are taken as immiscible. These assumptions leading to Eqs. (3)–(5) are implicitly contained in the constitutive relations of the mathematical model. Among other factors, the pressure field depends on the location of the injection and the production wells, the permeability distribution and the fluid viscosities.

In light of the observation that the pressure field stabilizes early in time (specifically, in 2–3 hours of injection time) its role in the evolution of the fingers is only indirect. An examination of Eq. (2) shows that the quantity of greater importance is the pressure gradient distribution over the physical domain.

The pressure gradient contours for isothermal injection in a homogeneous and a layered medium as in Fig. 4 are shown in Fig. 9(a), (b). The contour values have been normalized by the average gradient across the formation. They increase from left to right within a single plot, being the largest close to the production well. For a homogeneous region, the contours are symmetric about the main diagonal and change very slowly with time. The pattern seen at  $t = 33$  hours was also observed at an earlier time level of 3 hours. The corresponding contours for a layered medium (Fig. 9(b)) show pressure gradients set up parallel to the orientation of the porous layers. This is consistent with the tendency of the fluid to move along the high permeability zone of the formation. Pressure gradients in the low permeability zone are practically absent. These results correlate well with the saturation contours of Fig. 4.

Fig. 9(c), (d) show the normalized pressure gradient contours in a homogeneous and a layered medium (as in Fig. 4) for non-isothermal injection. The contours in the homoge-

neous region continue to be symmetric, consistent with the saturation contours of Fig. 6. The pressure gradients along the main diagonal remain small, suggesting that the displacement is more likely along the sides. The flow is however more vigorous, compared to isothermal injection; consequently the pressure gradients show a visible movement with time. The unsteadiness is more pronounced in the pressure gradients of the layered formation. The initial pattern at 5 hours was seen to be symmetric. At later times ( $t > 8$  hours) the contours get bunched in the high permeability zone, indicating the appearance of a finger. At 33 hours, one of the earlier patterns is reproduced, indicating the periodicity of the channeling phenomenon. At  $t = 50$  hours, the finger that reached the production well was followed by pinch-off.

The fingering phenomenon in a porous medium can create conditions under which the model assumptions are invalidated. Specifically, the channeling of water from the injection well to the production well and the appearance of pools of water from a pinched-off finger violate the assumptions that the fluid phases co-exist at all points in the physical domain. In numerical terms, a high water saturation can lead to a very low capillary pressure, thus destabilizing the entire calculation. In the present work, this factor restricted the integration time for non-isothermal injection to 33 hours.

## 5. Conclusions

Numerical simulation of oil–water flow in a porous formation has been reported in the present work. Homogeneous as well as layered formations have been considered. The influence of isothermal and non-isothermal injection on the displacement of oil and the formation of fingers has been studied. The following conclusions have been arrived at in the present work:

- (1) During isothermal injection in a homogeneous porous formation, the displacement process occurs radially outwards for the entire duration of simulation. At later times, a stable finger oriented along the diagonal joining the injection and the production wells is seen.
- (2) When hot water is injected, the initial displacement process is radially outwards, but at an increased speed. This leads to accumulation of oil ahead of the front and results in an increased resistance to front movement. Hence two lobe-like fingers emerge on the two sides of the physical domain. The flow patterns are symmetric at all times. The amount of oil recovered is consistently higher during non-isothermal injection. The saturation contours are seen to correlate well with those of temperature.
- (3) In a layered porous formation, the oil–water flow has been seen to respond strongly to the permeability distribution. There is a considerable difference in the response, depending on whether the high permeability zone is adjacent to the injection or the production well. In isothermal injection, the former arrangement is destabilizing with respect to the structure of the finger, while the latter is stabilizing. For non-isothermal injection, the finger is so dominant that the process is closer to channeling seen in fractured formations.

## References

- [1] R.E. Ewing, *The Mathematics of Reservoir Simulation*, SIAM, Philadelphia, PA, 1983.
- [2] P. Daripa, J. Glimm, B. Lindquist, Maesumi, O. McBryan, On the simulation of heterogeneous petroleum reservoirs, in: M.F. Wheeler (Ed.), *Numerical Simulation in Oil Recovery*, in: IMA Vol. Math. Appl., Vol. 11, Springer, Berlin, 1986, pp. 89–103.
- [3] C.T. Tan, G.M. Homsy, Simulation of nonlinear viscous fingering in miscible displacement, *Phys. Fluids* 31 (6) (1988) 1330–1338.
- [4] L.J. Durlofsky, R.C. Jones, W.J. Milliken, A nonuniform coarsening approach for the scale-up of displacement processes in heterogeneous porous media, *Adv. Water Resources* 20 (5–6) (1997) 335–347.
- [5] M.M. Dias, A.C. Payatakes, Network models for two phase flow in porous media—Part 1. Immiscible microdisplacement of non-wetting fluids, *J. Fluid Mech.* 164 (1986) 305–336.
- [6] R. Lenormand, E. Touboul, C. Zarcone, Numerical models and experiments on immiscible displacements in porous media, *J. Fluid Mech.* 189 (1988) 165–187.
- [7] E. Aker, K.J. Maloy, A. Hansen, G.G. Batrouni, A two-dimensional network simulator for two-phase flow in porous media, *Transport Porous Media* 32 (1998) 163–186.
- [8] T.C. Boberg, *Thermal Methods of Oil Recovery: An Exxon Monograph*, Wiley, New York, 1988.
- [9] H.R. Zhang, K.S. Sorbie, N.B. Tsibuklis, Viscous fingering in five-spot experimental porous media: new experimental results and numerical simulation, *Chem. Engrg. Sci.* 52 (1997) 37–54.
- [10] K. Aziz, Modeling of thermal oil recovery processes, in: W.E. Fitzgibbon (Ed.), *Mathematical and Computational Methods in Seismic Exploration and Reservoir Modeling*, SIAM, Philadelphia, PA, 1986, pp. 3–17.
- [11] M.D. Stevenson, M. Kagan, W.V. Pinczewski, Computational methods in petroleum reservoir simulation, *Comput. Fluids* 19 (1991) 1–19.
- [12] P.K.W. Vinsome, Fully implicit versus dynamic implicit reservoir simulation, *J. Canad. Petro. Tech.* (1985) 49–82.
- [13] T. Sheorey, K. Muralidhar, P.P. Mukherjee, Numerical experiments in the simulation of enhanced oil recovery, *Internat. J. Thermal Sci.* 40 (11) (2001) 981–997.
- [14] W.A. Hackbusch, Parallel conjugate gradient method, *J. Numer. Linear Algebra Appl.* 1 (2) (1992) 122–147.
- [15] B. Smith, P. Bjorstad, W. Gropp, *Domain Decomposition*, Cambridge University Press, Cambridge, 1999.
- [16] K.M. Pillai, K. Muralidhar, A numerical study of oil recovery using water injection method, *Numer. Heat Transfer* 24 (1993) 305–322.